International Journal of Thermophysics, Vol. 6, No. 6, 1985

Shear-Induced Melting and Reentrant Positional Ordering in a System of Spherical Particles[1]

S. Hess[2]

Computer simulations of dense systems of soft spheres subjected to a shear flow show not only the phenomena of shear-induced melting—transition from a crystalline to an amorphous state—but, at high shear rates, a second nonequilibrium phase transition to a new positionally ordered state. The particles form strings parallel to the stream lines; the strings, in turn, are arranged in a hexagonal pattern. Simulation data on the rheological properties, non-Newtonian viscosity, shear dilatancy, and stress growth and values for the shear moduli are presented; some theoretical ideas for the explanation of these phenomena are discussed.

KEY WORDS: nonequilibrium molecular dynamics; nonequilibrium positional ordering; nonlinear flow behavior; rheological properties; shear growth; shear-induced melting; shear moduli.

1. INTRODUCTION

The application of a shear to a solid can lead to the destruction of the crystalline order even under isothermal conditions. This shear-induced melting has recently been studied in colloidal crystals [1] with the help of light-scattering techniques and in nonequilibrium molecular dynamics simulations [2] for spherical particles. There are indications [1, 2] that the shear-induced melting does not proceed in one step if the shear rate is increased. In a certain range of shear rates, however, the system behaves as a dense fluid (amorphous system) which has "forgotten" that it can exist in a crystalline phase under equilibrium conditions. Thus it came as a surprise

[1] Invited paper presented at the Ninth Symposium on Thermophysical Properties, June 24–27, 1985, Boulder, Colorado, U.S.A.

[2] Institut für Theoretische Physik, Technische Universität Berlin, 1000 Berlin 12, Federal Republic of Germany.

0195-928X/85/1100-0657$04.50/0

(at least for the present author) that simple fluids—as studied in molecular dynamics—build up a (partial) positional order at high shear rates. The formation of planes parallel to the stream lines was noticed for both Lennard-Jones [3] and soft-sphere fluids [4]. The even more intriguing formation of strings of particles (parallel to the stream lines) which, in turn, arrange themselves in a hexagonal pattern has recently been observed for hard spheres [5] and, independently, for soft spheres [6, 7]. It should be mentioned that a somewhat similar reentrant positional ordering at high shear rates had previously been discovered experimentally for dense suspensions [8].

2. NONEQUILIBRIUM MOLECULAR DYNAMICS

In the following a fluid composed of "soft spheres" is considered, i.e., the binary interaction potential is

$$\Phi(r) = \varepsilon(s/r)^{12} \tag{1}$$

cut off at $r/s = 2.5$.

As usual, reduced variables are introduced with the help of the characteristic energy ε, the characteristic length s, and the mass m of a particle; e.g. densities n are expressed in units of s^{-3}, temperature T in units of εk_β (k_β is the Boltzmann constant), times in units of $t_0 = s(m/\varepsilon)^{1/2}$. For any power-law potential, the thermodynamic properties associated with the interaction potential do not depend on T and n separately. In the case of the potential given by Eq. (1), the relevant states variable is $X = (4T)^{-1/4}n$ [9]. In the simulations, the temperature $T = 0.25$ was chosen, thus $X = n$; T is kept constant by rescaling the magnitude of the (peculiar) velocities of the particles. At this temperature, a fluid with $n \approx 0.82$ coexists with a fcc solid with a density $n = 0.84$ according to Monte Carlo calculations [9]. The present studies were conducted for $n = 0.84$, i.e., at a "solid" density. The volume V of the system is determined by the prescribed number density n and the number of particles N; here the values $N = 2 \times 6^3 = 432$ and $N = 2 \times 4^3 = 128$ were chosen. Periodic boundary conditions are used. The equations of motion are integrated with a fifth-order predictor-corrector method (Gear).

In the nonequilibrium MD (NEMD), a plane Couette flow with the velocity field

$$v_x = \gamma y, \qquad v_y = 0, \qquad v_z = 0 \tag{2}$$

and the constant shear rate

$$\gamma = \frac{\partial V_x}{\partial y} \tag{3}$$

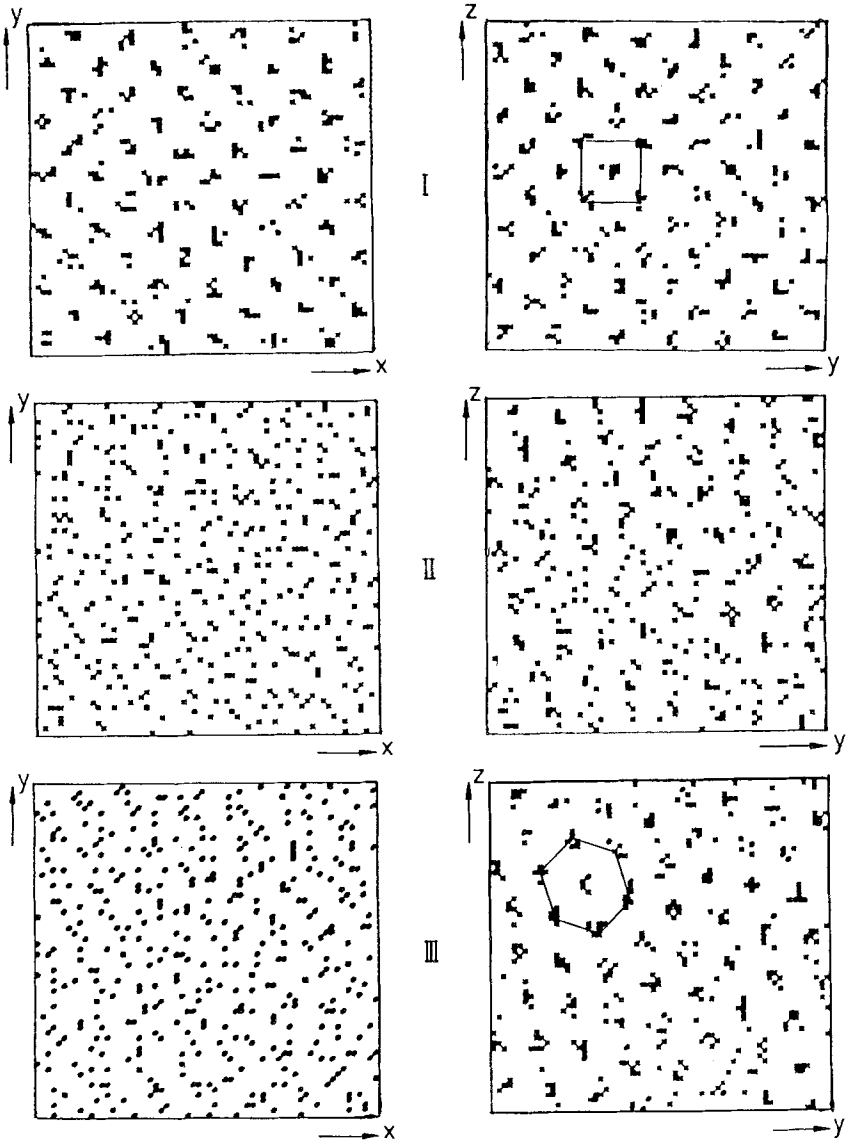

Fig. 1. Projections of the positions of the particles on walls parallel to the shear plane (x–y plane) and perpendicular to the flow velocity (y–z plane), respectively. The snapshot pictures were taken in the unsheared bcc phase (I), at an intermediate shear rate (II), and at a high shear rate in the string-ordered phase (III).

is simulated by controlling the velocity gradient tensor. The method is essentially equivalent to one described by Evans [10]. Of course, in the presence of a flow, the periodic boundary conditions have to be modified appropriately. The time steps are of length 0.01 in most cases; for high shear rates shorter time steps were required. The program has previously been tested for nonequilibrium studies in Lennard-Jones and soft-sphere systems at other state points [4, 6, 11–13].

3. THE NONEQUILIBRIUM PHASE TRANSITIONS

Next, consider Fig. 1 for a demonstration of the shear-induced melting and the reentrant positional ordering in the 432-particle system. The "snapshot" pictures on the left-hand side in of Fig. 1 are projections of the positions of the particles in the volume V on the x–y plane (shear plane); those on the right-hand side are projections on the z–y plane, which is perpendicular to the flow direction, i.e., one "looks" upstream or downstream. The first two graphs (marked I) show the system in the initial bcc solid phase. The snapshot was taken 500 time steps after the start; no shear has been turned on yet. At the density $n = 0.84$ the bcc phase seems to be metastable. The application of a (small) shear destroys the crystalline order: shear-induced melting. The graphs marked II in the middle of Fig. 1 show the state of the system flowing with an intermediate shear rate $\gamma = 0.5$; the appearance is fluid-like, although the picture on right shows some indications of tilted layers. The graphs labeled III are for the shear rate $\gamma = 2.0$; the system had been subjected to this shear rate for 1600 time steps. The projection onto the y–z plane reveals that the particles are moving (cooperatively) in strings which, in turn, try to maximize their distances. This gives rise to the hexagonal pattern. The sides of the hexagons are tilted with respect to the periodicity box; for this reason one does not see the ordering in the shear plane. In the following, this new phase is referred to as the "string-ordered state."

The same two nonequilibrium phase transitions were observed in the $N = 128$ particle system. Since the thermophysical properties analyzed at three shear rates γ were quite similar for $N = 432$ and $N = 128$, most runs (at 12 values of γ) were performed for the smaller system.

4. COMPARISON BETWEEN THE SOLID AND THE FLUID STATE

To investigate the difference between the (metastable) bcc phase and the amorphous fluid after shear-induced melting, the mean square displacement R^2 was determined for both cases. In Fig. 2, $\frac{1}{3}R^2$ is plotted as a function of the time t (for the $N = 128$-particle system). Curve 1 is for the

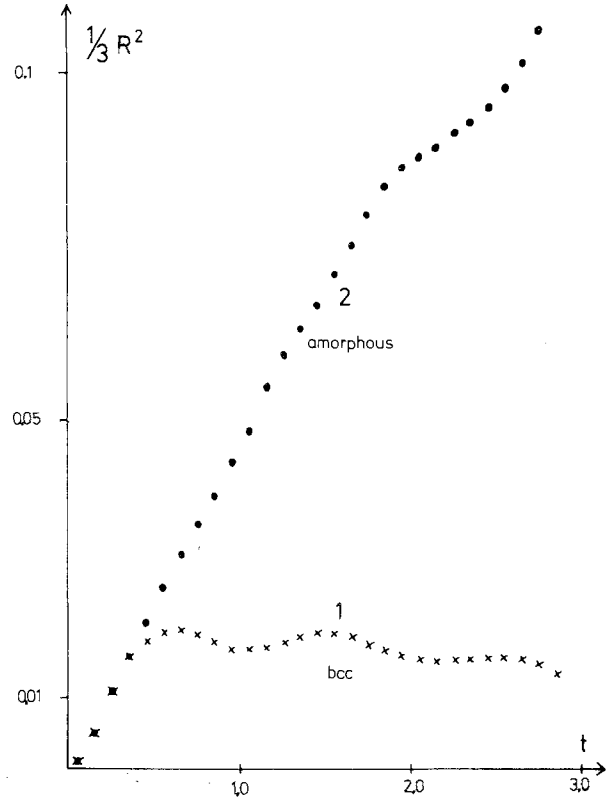

Fig. 2. One-third of the mean square displacement R^2 as function of the time t. Curves 1 and 2 pertain to the bcc phase and the amorphous phase after shear-induced melting, respectively.

bcc phase; $t=0$ correponds to 200 time steps after the initial start of the simulation. Curve 2 pertains to the case where the system has undergone a shear-induced melting. More specifically, a flow with the shear rate $\gamma=0.125$ was going on for 1000 time steps before the shear rate was switched off and the calculation of R^2 was started. Clearly, there is a marked difference between both cases. The saturation of R^2 for large times and the growth of R^2 proportional to t are typical for a solid and a fluid, respectively.

Of course, there are also differences in the thermophyscial properties. In Table I, the potential contributions to the pressure P, the compressibility modulus K, the shear (isotropic) modulus G, the cubic shear modulus G_c, and the square of the Einstein frequency are listed. All quantities are evaluated as N-particle averages (and they have been averaged

Table I. The Potential Contributions to the Thermodynamic Functions P, K, G, and G_c and the Square of the Einstein Frequency ω_E for the bcc Phase and the Amorphous Fluid Phase After Shear-Induced Melting

	P	K	G	G_c	ω_E^2
bcc	3.82	19.09	6.87	−6.56	81.8
Fluid	4.30	21.51	7.74	−0.16	95.2

over 200 time steps) with the help of formulas which are standard except for G_c [14].

The shear modulus G, in particular, is given by

$$G = n \sum_{i \neq j} \sum A(\mathbf{r}_{ij}) \tag{4}$$

where n is recalled as the number density, $\mathbf{r}_{ij} = \mathbf{r}_i - \mathbf{r}_j$ is the difference in the position vectors of particles i and j, and the quantity $A(\mathbf{r})$ stands for

$$A(\mathbf{r}) = \frac{1}{30} r^{-2} (r^4 \phi')' \tag{5}$$

The prime denotes the derivative with respect to r. The cubic modulus G_c is given by an expression analogous to Eq. (4), but with A replaced by

$$A_c(\mathbf{r}) = \frac{5}{24} H_4(\hat{\mathbf{r}})\, r^3 (r^{-1} \phi')' \tag{6}$$

$$H_4(\hat{\mathbf{r}}) = \hat{x}^4 + \hat{y}^4 + \hat{z}^4 - 3/5 \tag{7}$$

is a cubic harmonic. In Eq. (7) $\hat{x}$, $\hat{y}$, and $\hat{z}$ are the components of the unit vector $\hat{\mathbf{r}}$ with respect to the coordinate axes, which are assumed to be parallel to the cubic axes. For a system with cubic symmetry the Voight elasticity coefficients c_{ik} are related to the quantities K, B, and G_c by

$$c_{11} = c_{22} = c_{33} = K + \frac{4}{3} G + \frac{4}{5} G_c \tag{8}$$

$$c_{12} = c_B = c_{23} = K - \frac{2}{3} G - \frac{2}{5} G_c \tag{9}$$

$$c_{44} = c_{55} = c_{66} = G - \frac{2}{5} G_c \tag{10}$$

For an isotropic (fluid or amorphous) system K and G are nonzero, but

$$G_c = \frac{1}{2}(c_{11} - c_{12}) - c_{44} \tag{11}$$

vanishes. Thus G_c is an excellent indicator for a crystalline order (of cubic symmetry) (cf. Table I).

Incidentally, for a power-law potential, the potential contributions to P, K, and G are not independent; e.g., one has

$$G = \frac{9}{5}P \tag{12}$$

Similarly $K = 5P$ and $P = 4nU$ for the $r - 12$ potential given by Eq. (1); U is the potential contribution to the internal energy per particle. The kinetic contributions to P, K, and G are nT; G_c has no kinetic part.

5. RHEOLOGICAL BEHAVIOR AND SHEAR-INDUCED ORDERING

5.1. Pressure Tensor, Viscosity

The pressure tensor $\mathbf{P}$ of a system of N spherical particles is the sum of the kinetic and the potential parts

$$\mathbf{P} = \mathbf{P}^{\text{kin}} + \mathbf{P}^{\text{pot}} \tag{13}$$

which in a simulation, in contradistinction to a real experiment, can be recorded separately. The standard formulas used for the evaluation are

$$\mathbf{P}^{\text{kin}} = V^{-1} \sum_i \mathbf{c}^i \mathbf{c}^i \tag{14}$$

$$\mathbf{P}^{\text{pot}} = V^{-1} \frac{1}{2} \sum_{i \neq j} \sum \mathbf{r}^{ij} F^{ij} \tag{15}$$

Here, V is the volume; $\mathbf{c}^i$ is the peculiar velocity of particle i, i.e., its velocity with respect to the average flow velocity; and $\mathbf{F}^{ij} = \mathbf{F}(\mathbf{r}^{ij})$, with $\mathbf{F}(\mathbf{r}) = -\partial \Phi / \partial \mathbf{r}$ is the foce between particle i and particle j.

In general, the tensor $\mathbf{P}$ can be decomposed into an isotropic part $P\boldsymbol{\delta}$, where $\boldsymbol{\delta}$ is the unit tensor, and an symmetric traceless (anisotropic) part $\mathbf{p}$, which vanishes in thermal equilibrium. The "scalar" part P of the pressure is one-third of the trace of $\mathbf{P}$; the quantity P listed in Table I corresponds to P^{pot} as inferred from Eq. (15).

For the plane Couette symmetry considered here [cf. Eqs. (2) and (3)], the non-Newtonian viscosity $\eta = \eta(\gamma)$ is defined by

$$p_{xy} = -\eta(\gamma)\gamma \tag{16}$$

In the nonlinear flow regime, the scalar pressure $P = 1/3(P_{xx} + P_{yy} + P_{zz})$ also depends on the shear rate γ, and there are normal pressure differences [15, 16]. Here the attention is focused on the non-Newtonian viscosity, Eq. (16).

In Fig. 3 the magnitude of p_{xy} is plotted as a function of the shear rate γ; the squares and the circles mark the potential and 10 times the kinetic contributions to the x–y component of the pressure tensor. The lines between the data points are intended as a guide for the eye. Notice the break in the curve for $p_{xy}{}^{pot}$ and the change in the slope at a shear rate of about $\gamma = 2$ associated with the flow-induced transition into the string-ordered state discussed above. The data were averaged over 2000 to 4000 time steps; for details see Table II. Strong fluctuations were observed for $\gamma = 2$; the three different data points stem from consecutive runs of at least 2000 time steps.

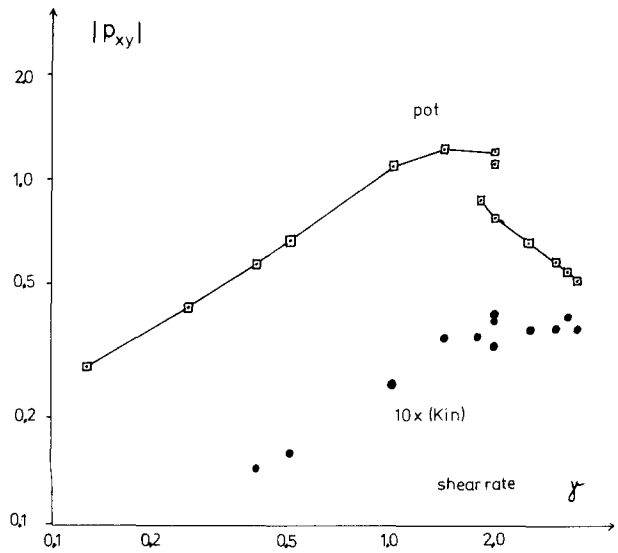

Fig. 3. The magnitude of the x–y component p_{xy} of the pressure tensor as a function of the shear rate γ. The squares and the circles mark the potential and (10 times) the kinetic contributions, respectively. The lines are intended as a giode for the eye.

Table II. The Same Quantities as in Table I Plus the Kinetic and Potential Contributions to the x–y Component of the Pressure Tensor as Well as the Entropy Production $\dot{S}$ for Various Shear Rates γ[a]

	T	γ	tst	P^{pot}	K^{pot}	G^{pot}	G_c	W_E^2	$-p_{xy}^{kin}$	$-p_{xy}^{pot}$	$\dot{S}$
1	0.2501	0.1248	3000	4.36	21.8	7.85	-0.44	96.0	0.003	0.285	—
2	0.2508	0.2502	3400	4.50	22.5	8.10	0.20	101.0	0.008	0.434	0.47
3	0.2517	0.3999	2400	4.58	22.9	8.26	0.50	103.0	0.014	0.57	1.04
4	0.2527	0.5002	2000	4.96	24.8	8.45	0.36	106.0	0.016	0.70	1.70
5	0.2587	1.000	3100	5.06	25.3	9.12	0.92	117.0	0.025	1.09	5.20
6	0.2641	1.414	2500	5.30	26.5	9.54	2.01	125.0	0.035	1.23	8.47
7	0.2629	1.800	1000	5.06	25.3	9.11	4.6	117.0	0.035	0.87	7.72
8a	0.2682	2.000	2000	5.36	26.8	9.65	4.7	127.0	0.040	1.11	11.0
8b	0.2697	2.001	3100	5.42	27.1	9.76	4.2	129.0	0.041	1.20	11.8
8c	0.2642	2.000	3000	4.98	24.9	8.97	5.1	115.0	0.034	0.78	7.7
9	0.2639	2.505	2100	4.97	24.7	8.89	6.6	115.0	0.037	0.66	8.35
10	0.2651	3.000	2100	4.98	24.9	8.96	7.14	115.0	0.038	0.58	9.15
11	0.2635	3.200	2000	5.06	25.3	9.11	4.60	118.0	0.041	0.56	9.31
12	0.2540	3.500	4500	4.95	24.7	8.91	7.35	114.3	0.036	0.51	9.57

[a] The prescribed temperature is 0.25 in all cases; the column T gives the observed temperature. tst indicates the number of time steps over which the data have been averaged.

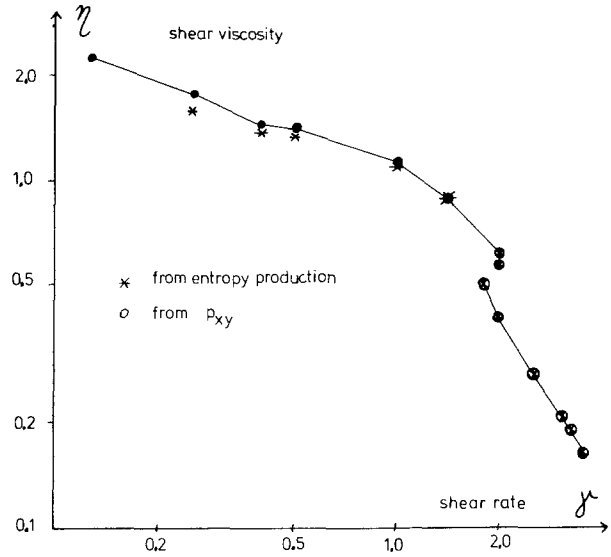

Fig. 4. The non-Newtonian viscosity η as function of the shear rate γ. The cirles are for data obtained from p_{xy}; the asterisks are inferred from the entropy production.

The non-Newtonian viscosity $\eta(\gamma)$ is displayed in Fig. 4. The circles are obtained from the sum of the kinetic and potential contributions to p_{xy}; cf. Eq. (16). The crosses are inferred from the entropy production $\dot{S}$ (per particle) according to

$$\dot{S} = (nT)^{-1} \eta(\gamma) \gamma^2 \tag{17}$$

In the simulation, the quantity $\dot{S}$ is essentially evaluated from the heat which is extracted from the system in order to keep the temperature constant. Clearly, there is an excellent agreement between both methods unless the shear rate γ is too small, where statistical fluctuations affect the second method more strongly. Again, notice the break in the curve and the change in the slope at about $\gamma = 2$.

The viscosity η is strongly non-Newtonian even for $\gamma < 2$, where the system is in the amorphous fluid state. In fact, it is not possible to determine a Newtonian limit for η because there is no region where p_{xy} increases proportionally to γ in the range of γ studied here. This is in contradistinction to simulations performed for smaller densities [6, 16, 17]. The previously tested functional from $\eta(\gamma) = \eta(0)(1 - a_1 \gamma^{1/2})$ with a coefficient a_1 does not fit the data. In the range $0.1 < \gamma < 1.5$ one finds,

approximately, $-p_{xy} \sim \gamma^{2/3}$ and, consequently, $\eta \sim \gamma^{-1/3}$. In the string-ordered state ($1.8 < \gamma \lesssim 3.5$) $-p_{xy}$ decreases like γ^{-1}, here $\eta \sim \gamma^{-2}$; this implies $\dot{S} \approx$ const [cf. Eq. (17)]. Since no theoretical foundation can be given for these power laws, they should be understood just as "empirical" expressions. However, the main points to be made in this section are clearly revealed by these considerations: there is a strong non-Newtonian shear thinning flow behavior in the amorphous fluid state, and the (first order) nonequilibrium phase transition to the string-ordered state at high shear rates drastically affects the rheological properties of a fluid a solid densities.

For dimensional reasons, the dependence of η (and of other quantities) on γ must be via $\gamma\tau$, where τ is a characteristic relaxation time, e.g., the ratio between the viscosity η_{New} and the shear modulus G in the Newtonian limit. It has been noticed in simulations for soft-sphere and Lennard-Jones systems at other state points that τ is somwhat larger (by a factor about 2) but of the same order of magnitude as the reciprocal Einstein frequency ω_E^{-1} in equilibrium fluids. With $G \approx 7.7$ and $\eta_{\text{New}} > 2.3$ one has $\tau > 0.3$ for the present case; on the other hand, one finds $\omega_E^{-1} \approx 0.1$ and, consequently, $\tau\omega_E > 3.0$. This is in accord with an extrapolation of an empirical formula for the density dependence of η_{New} proposed by Ashurst and Hoover [17], which yields $\eta_{\text{New}} = 2.9$ for $n = 0.84$. This leads to $\tau \approx 0.35$ and $\tau\omega_E \approx 3.5$.

The potential contribution to the scalar part $P = 1/3(P_{xx} + P_{yy} + P_{zz})$ of the pressure tensor increases with increasing shear rate: shear dilatancy. Due to the relation given by Eq. (12), the dependence of P on γ can be inferred from that of the shear modulus G, discussed next. The kinetic contribution to P is constant since the density n and the temperature T are kept constant.

5.2. Shear Moduli

In Fig. 5, the isotropic and the cubic shear moduli G and G_c are displayed as functions of the shear rate. These coefficients characterize the elastic behavior for a small volume conserving deformation; G_c is intimately linked with the cubic symmetry (cf. Eqs. 4–7), i.e., it vanishes in anisotropic fluid in equilibrium. In the ordinary fluid phase, G increases with increasing shear rate. In the string-ordered state, there is a drop to a somewhat smaller value and G seems to stay constant. Due to $G \sim P$, this reflects the fact that the pressure stays constant over a certain range of values for the shear rate γ. Such a behavior is indicative of a first-order phase transition.

The cubic shear modulus G_c shows a small increase at small shear rates ($\gamma \lesssim 1$), then a steep rise to larger positive values for $\gamma \geqslant 2$. Notice that

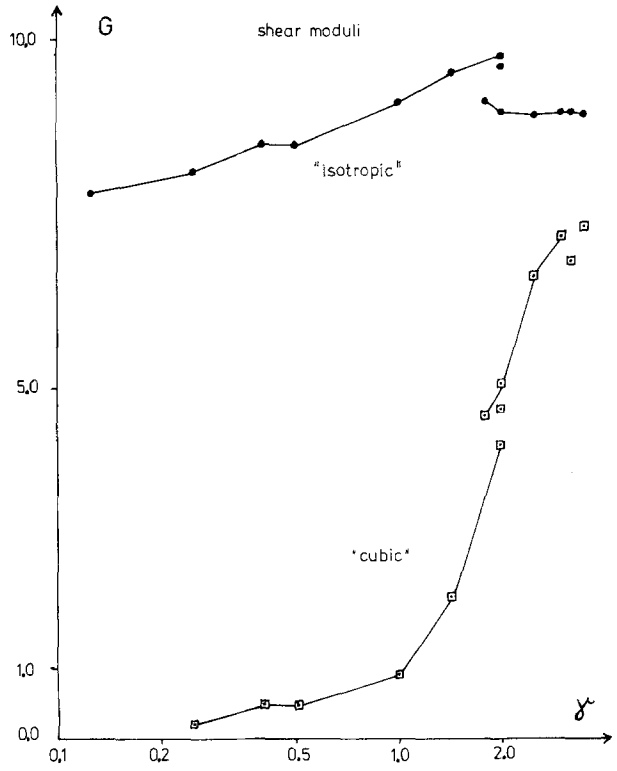

Fig. 5. The potential contribution to the "isotropic" shear modulus G (filled circles) and the "cubic" shear modulus G_c (squares) as a function of the shear rate $\dot{\gamma}$.

the magnitude of G_c in the flow-induced ordered state is about as large as in the equilibrium bcc state; the sign, however, is different (in both the bcc and the fcc phase, G_c is negative). This can be understood as follows. The radial part of the quantity A_c [cf. Eq. (16)], needed for the evaluation of G_c, is positive and proportional to r^{-12} in the present case. Thus the sign of G_c is determined by the sign of the cubic harmonic $H_4(\hat{\mathbf{r}})$ [cf. Eq. (7)], where $\hat{\mathbf{r}}$ is the unit vector pointing from a reference atom to the first neighbors. In the solid bcc and fcc phases, these are along the body or face diagonals where $H_4(\hat{\mathbf{r}})$ is negative. In the flow-induced ordered state (see Fig. 1), there is a high chance to find nearest neighbors along the x direction and also along the y and z directions where $H_4(\hat{\mathbf{r}})$ is positive. Thus, G_c is an excellent indicator for a "bond directional" order [11]. Notice, however, that the flow-induced string-ordered state does not have a cubic symmetry.

5.3. Stress Growth

The formation of a new phase takes time. This also applies to the non-equilibrium phase discussed here, and it is reflcted in the stress growth curves displayed in Fig. 6. The magnitude of (the potential contribution t_0) p_{xy} is plotted as a function of the time after the time $t=0$ where the shear rates $\gamma=0.4$, $\gamma=1.8$, and $\gamma=3.2$ were switched on; the three curves are labeled by these values for γ. All three runs started from the same amorphous state, where the system had undergone a shear flow with $\gamma=0.125$ for 1000 time steps. For all shear rates, there is a fast increase in p_{xy} over the time interval $t \lesssim 2$, corresponding to 200 time steps. For $\gamma=0.4$, the final value is practically reached after this time. Since the data are time averaged over 100 time steps only, the curves show statistical fluctuations. For $\gamma=3.2$, there is a pronounced stress overshoot. The drop in p_{xy} from $t=2$ to about $t=10$ is associated with the formation of the flow-induced ordered state. The final values of p_{xy} are about the same for $\gamma=0.4$ and $\gamma=3.2$ (cf. Fig. 3). At the intermediate value $\gamma=1.8$, one still observes a stress overshoot, but

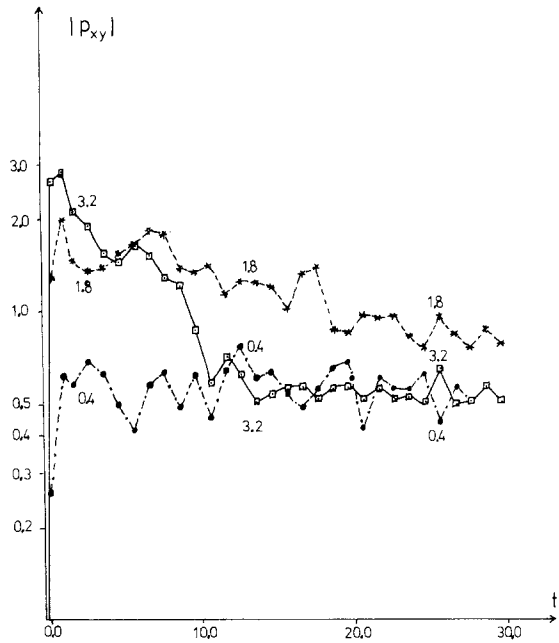

Fig. 6. Stress growth curves for the shear rates $\gamma=0.4$ (dashed–dotted line), $\gamma=1.8$ (dashed line), and $\gamma=3.2$ (solid line). Notice the stress overshoot for the two larger values of γ.

the decay of p_{xy} to its final value is much slower since it is close to the critical value where the transition to the string-ordered state sets in.

The hexagonal pattern of the string-ordered state must fit into the periodicity box. Thus the time of formation of the new phase is expected to depend on the size of the system, i.e., on N, even when thermophysical properties in the stationary state are practically independent of N. This has indeed been noticed in a comparison of the $N = 432$- and $N = 128$-particle simulations for $\gamma = 2$; for $\gamma \leqslant 1$ there are only small differences.

5.4. Further Observations on the String-Ordered State

In the nonlinear flow regime, one has normal pressure differences, which for the present geometry are best characterized by the two quantities $p_- = 1/2(P_{xx} - P_{yy})$ and $p_0 = 1/2[P_{zz} - 1/2(P_{xx} + P_{yy})]$. Together with $p_+ = P_{xy}$, these are the three of the five components of the symmetric traceless pressure tensor which are nonzero, in general, for the plane Couette symmetry [6, 12, 16]. In the simulations discussed here, the statistical accurracy is not good enough to present data on the quantities p_- and p_0, which are typically at least one order of magnitude smaller than p_+. However, the qualitative observation that the potential contributions to p_- and p_0 are negative in the amorphous fluid state (in accord with data obtained at lower densities) but positive in the string-ordered state deserves mentioning. Furthermore, it is remarkable that the Couette symmetry is broken in the new phase; in particular, p_{zy} becomes nonzero. This is probably associated with squeezing the hexagonal pattern (cf. Fig. 1) into a square determined by the periodicity box.

A technical detail may be worth mentioning. In the string-ordered state, it is not possible to change the shear rate without drastically decreasing the length of the time steps Δt. However, the same values of the shear rate can be reached without any problem (i.e., with $\Delta t = 0.01$) from the amorphous fluid state (cf. Fig. 6).

6. CONCLUDING REMARKS

The nonequilibrium molecular dynamics simulations for a soft-sphere system at a solid density demonstrate that (at least) two nonequilibrium phase transitions occur with increasing shear rate: first, the shear-induced melting and, second, the formation of a reentrant positionally ordered state where strings of particles are arranged in a hexagonal pattern. The theoretical treatment of these phase transitions and of the complex rheological behavior of such a system is quite a challenge.

The problem of shear-induced melting and the influence of a viscous

flow on the phase transition fluid–solid has recently been studied [18] by a theoretical approach where the two phases are distinguished by a bond-orientational order parameter tensor (of rank 4). An equation of change for this quantity was derived from a generalized Fokker-Planck equation where viscous torques on the bond direction were taken into account.

The transition from the fluid to the string-ordered state poses even more challenges for a theoretical explanation. As a first step it may be useful to exploit formal analogies between the potential contribution to the symmetric traceless friction pressure tensor **p** of a simple fluid and the second-rank alignment tensor **a** of a nematic liquid crystal where a shear-induced phase transition has been studied before [19]. The first quantity, to some extent, specifies the bond-directional orientation, i.e., the preferential orientation of a vector joining two correlated spherical particles; the latter one describes the orientation of the long axis of a molecule. For the characterization of the string-ordered phase, in addition to the (second-rank) pressure tensor, however, a further order parameter is needed to specify the hexagonal packing of the strings, which is similar to the order within one layer of a liquid crystal of type smectic *B*.

Finally, it should be stressed that the soft-sphere system, as academic as it seems at first glance, shows many nonequilibrium phenomena found in dense suspensions of spherical particles.

REFERENCES

1. B. J. Ackerson and N. A. Clark, *Physica* **118A**:221 (1983).
2. D. J. Evans, *Phys. Rev.* **A25**:2788 (1981).
3. D. M. Heyes, J. J. Kim, C. J. Montrose, and T. A. Litovitz, *J. Chem. Phys.* **73**:3987 (1980).
4. S. Hess, *Proc. Colloidal Crystals* (Les Houches, 1984); *J. de Physique* **46**:C3–191 (1985).
5. J. J. Erpenbeck, *Phys. Rev. Lett.* **52**:1333 (1984).
6. S. Hess, *JMTA*.
7. H. J. M. Hanley, Private communication.
8. R. L. Hoffmann, *Trans. Soc. Rheol.* **16**:155 (1972).
9. W. G. Hoover e. a., *J. Chem. Phys.* **52**:493 (1970).
10. D. J. Evans, *Mol. Phys.* **37**:1745 (1979).
11. S. Hess, *Physica* **127A**:509 (1984).
12. S. Hess, H. J. M. Hanley, and N. Herdegen, *Phys. Lett.* **105A**:238 (1984).
13. S. Hess, *Phys. Lett.* **105A**:113 (1984).
14. S. Hess, In press.
15. D. J. Evans, H. J. M. Hanley, and S. Hess, *Phys. Today* **37**:26 (1984).
16. S. Hess and H. J. M. Hanley, *Int. J. Thermophys.* **4**:77 (1983).
17. W. T. Ashurst and W. G. Hoover, *Phys. Rev.* **A11**:658 (1975); W. G. Hoover, *Physica* **118A**:111 (1983).
18. N. Herdegen, *Influence of a Shear Flow on the Phase Transition Liquid-Solid*, Thesis (University of Erlangen-Nürnberg, 1984).
19. S. Hess, *Z. Naturforsch.* **31a**:1507 (1976).